




Scalable deposition of sol–gel based monolayer antireflective thin films by using a dual alkoxysilane precursor chemistry

Gizem Aydın Sobacı¹ · Osman Burak Okan¹ · Kürşat Kazmanlı² · Refika Budakoğlu ¹

Received: 1 October 2021 / Accepted: 11 April 2022 / Published online: 7 May 2022

© The Author(s), under exclusive licence to Springer Science+Business Media, LLC, part of Springer Nature 2022

Abstract

In this study, we investigate the prospect of using dual alkoxysilane precursor chemistry for the scalable deposition of antireflection thin films on soda lime silicate glass. The hybrid chemistry involves the use of tetraethyl orthosilicate (TEOS) in combination with methyltriethoxysilane (MTES). Throughout the study, we use a dual acidic catalyst system comprising an organic (acetic acid) and an inorganic (nitric acid) acid. After the coating process, the coated glasses are cured at 100 °C and then annealed at 700 °C to mimic a typical industrial tempering process. The effects of altering the MTES/TEOS mole ratio on the resulting colloidal sol are studied with five different sols using Fourier Transform Infrared (FTIR) analysis and the final properties of solid thin films are investigated in detail through optical spectrophotometry, contact angle measurements, optical microscopy and electron microscopy (Scanning Electron Microscopy (SEM) and Scanning Transmission Electron Microscopy (STEM)) techniques. In addition to the coated glasses, we investigate the thermal stability of dried gels at room conditions as well as at 100 °C, 400 °C, and 700 °C annealing temperatures. Since the PV panel glasses are typically deployed to stay in contact with the external environment, the weathering durability of the samples having optimum properties are investigated in accordance with EN 1096-2 and IEC 61215 standard test methods. It is shown that the presented dual precursor chemistry can produce coatings that exhibit high mechanical and chemical resistance and retain their anti-reflective properties when treated with an industrial tempering process. Finally, we provide evidence that laboratory scale dip coating process can be directly scaled up to a roller coating process without compromising optical performance. Our results show that commercial solar module dimensions and patterned glasses can be directly accommodated with the proposed coating chemistry.

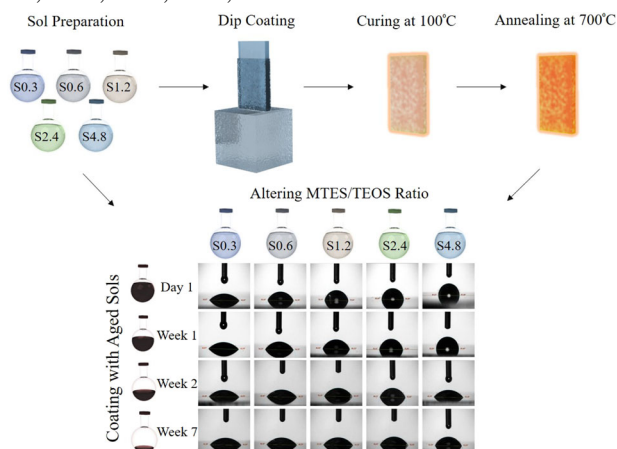
✉ Refika Budakoğlu
rbudakoglu@sisecam.com

² Department of Metallurgical and Material Engineering Istanbul Technical University, Istanbul, Turkey

¹ Atmospheric Coating Technologies Division Sisecam Science Technology and Design Center, Kocaeli, Turkey

Graphical Abstract

Sample preparation process flow chart and contact angle measurements of coated samples which were cured at 100 °C and then annealed at 700 °C using S0.3, S0.6, S1.2, S2.4, and S4.8 solutions with different time intervals.



Keywords Anti-reflective · Silica · Sol-gel · Thin films

Highlights

- Highly durable monolayer anti-reflective (AR) coatings that can be annealed with an industrial tempering process up to 700 °C are demonstrated.
- Using a dual precursor chemistry based on tetraethyl orthosilicate (TEOS) and methyltriethoxysilane (MTES) highly durable AR coatings are obtained and are tested according to EN1096-2 and IEC 61215 standards.
- In the presence of a dual acid catalyst system, changes in MTES/TEOS molar ratio fundamentally affect the durability of the AR coatings.
- Coating with sols aged up to 7 weeks allows us to demonstrate the long-term stability of the coating chemistry.
- Using an industrial grade roll coater, we show that the proposed coating chemistry can be directly scaled-up.

1 Introduction

Thin-film antireflection (AR) coatings operate with the physical principle of thin film interference whereby a single or multilayer thin film stack eliminates the reflections at the substrate-air interface [1, 2]. Depending on the target application and process constraints such as deposition chemistry, thickness control, or allowable substrate size sol-gel based atmospheric methods or vacuum deposition methods can be used [3]. For Si based photovoltaic systems typically, single layer low refractive index thin film layers of 90–120 nm thickness are used for AR purposes [4]. The target thickness can be chosen to match the peak solar spectral radiance or the total solar spectral radiance curve between 400 and 1100 nm where the crystalline Si PV modules function [5]. In this study, we use the former approach. On a soda lime glass whose refractive index is about 1.52, thin films with a refractive index of 1.23 are ideally needed (ignoring the slight wavelength dependence of the refractive indices) but there is no naturally occurring material with such a low index of refraction. An alternative and well-established route are to deposit thin oxide

films with reduced density through introducing structural voids [6–8]. Carefully nanostructured broadband AR coatings can attain extremely low refractive with more advanced deposition techniques [9, 10]. However, there is an unavoidable trade-off between layer porosity and durability. In photovoltaic applications, materials with very high porosity would lack the desired weathering resistance and scalability for large area coating applications.

Thin-film coatings can possess either closed or open pore topology and if pore size is much smaller than the target wavelength the material acts as a homogenous material with a much lower refractive index. Coatings with closed pore topology are less prone to environmental effects but entail a more complex synthesis route [11–13]. Thin film structures with open pore topology can also produce functional AR coatings. However, unmodified SiO₂-based coatings with open pore topology are susceptible to optical breathing which increases the refractive index thus reducing transmission [14, 15]. Chemical modification of the silica sols is known to alleviate this shortcoming through improved hydrophobicity [15, 16]. Cai et al. use a two-step base/acid catalytic synthesis

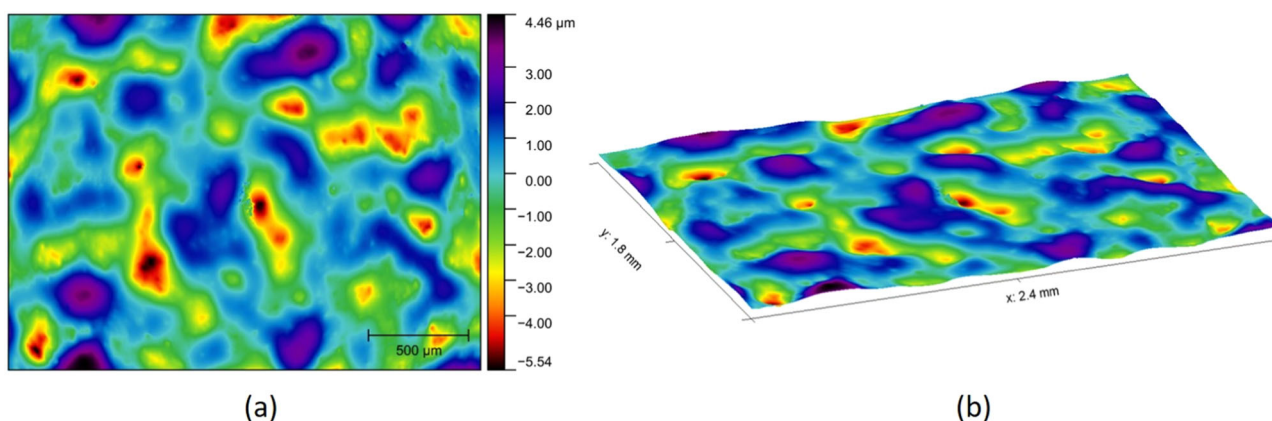


Fig. 1 WLI imaged surface topography of patterned glass: **(a)** surface contour map **(b)** 3D surface plot of the same image. Both images feature the same color coding of height data. This image was plotted

with GWYDDION software using the raw data from the WLI measurement after flattening of base [33]

route to obtain AR coatings based on surface modified SiO_2 particles cladded with methyl groups that offer high humidity resistance and high optical transmission [15]. There are more recent studies that rely on the aggregation of silica nanoparticles synthesized with the Stöber method [17, 18]. Lin et al. discusses organic modified silica coatings which are obtained by the combined use of phenyltriethoxysilane (PTES) and TEOS [17] and Chi et al. improve the stability of the silica based AR coatings by imparting a hydrophobic character through exposure to hexamethyldisilazane [18]. In a similar study, a vapor phase treatment with hexamethyldisilazane is noted for improving weathering resistance [19]. However, in these studies, the high temperature stability of the resulting coatings is not addressed.

In this study, we present a simple single step chemical route to attain SiO_2 based thin films that are highly durable. These layers can be homogeneously coated on macroscopically patterned glass substrates in a single coating step followed by a thermal annealing treatment at 700°C . This particularly high annealing temperature exceeds the previous studies, but it was deliberately chosen to be compatible with industrial thermal tempering process commonly used for the strengthening cover glasses in Si based modules. Using MTES, an organo-alkoxysilane bearing a methyl group, in combination with TEOS allows us to alter the wettability of the AR coating and minimize transmission losses due to water adsorption. We present a detailed account of long-term durability of high-temperature annealed AR coatings as well as the thermal stability of methyl modification of the silica network in dried gels.

2 Experimental procedure

Anti-reflective thin film coatings were obtained by changing the molar ratios of MTES/TEOS in the presence of an acidic

catalyst system comprising an organic (acetic acid) and an inorganic acid (nitric acid). Acetic acid is a weak electrolyte and has been noted for its role as a peptization agent with superior wetting properties in the preparation of transparent alumina systems [6, 20]. The use of acetic acid has the additional benefit (not elaborated here) of limiting the corrosion on industrial roll coating systems where austenitic stainless-steel components are typically used. Nitric acid is chosen because, when combined with acetic acid, it markedly increases the weathering resistance of the coatings, most notably in salt spray testing. Coating sols were obtained by one-pot co-condensation of two precursors which were TEOS ($\text{Si}(\text{OC}_2\text{H}_5)_4$, Evonik Industries AG) and MTES ($\text{CH}_3\text{Si}(\text{OC}_2\text{H}_5)_3$, Evonik Industries AG) with different proportions in the presence of deionized water, acetic acid (CH_3COOH , HAc, Merck 100%), nitric acid (HNO_3 , Merck 65%), ethanol (EtOH, Sigma Aldrich 96%), propan-2-ol (IPA, Sigma Aldrich 99.8%), and propylene glycol monomethyl ether acetate (PMA, Mikro Teknik 99.9%). These chemicals were used as received without further purification. The molar ratios of MTES/TEOS were varied from 0.3 to 4.8 by doubling the ratio of MTES/TEOS for each case. The solutions were prepared in deionized water with a water/alkoxy (R) ratio of 2. The overall molar ratio was $\text{TEOS}:\text{MTES}:\text{H}_2\text{O}:\text{HAc}:\text{HNO}_3:\text{EtOH}:\text{IPA}:\text{PMA} = x:y:10:3:0.0002:12:68:1$ and has been previously described elsewhere [21]. Throughout the experiments, the solutions were stored in sealed glass containers at room temperature.

Şişecam's 3.2 mm commercial grade patterned solar glasses of soda lime composition with a 140 ± 20 ppm iron content (Rigaku Primus II XRF, Japan) were used as substrates. The surface is characterized by average roughness values in absolute and root mean squared sense with $R_a = 1.12 \mu\text{m}$ and $R_q = 1.39 \mu\text{m}$, respectively [22]. The surface topography of a sample patterned glass is presented in Fig. 1.

Table 1 Sample codes of solutions according to the molar ratio of MTES/TEOS

Sample codes	S0.3	S0.6	S1.2	S2.4	S4.8
Molar ratios of MTES/TEOS	0.3	0.6	1.2	2.4	4.8

The surface data were acquired with WLI (White Light Interferometry) by using a Contour GT-K 3D optical profilometer (Bruker Corporation, Germany) at 2.5 magnification.

During this study, flat glass samples were subjected to multistep washing and drying processes, respectively, prior to the coating operation. Washing steps were carried out in a washing machine (FinnSonic WV-120/90, Finland). This device consists of 5 separate tanks stacked in tandem. The first tank contains a basic solution containing 3–10% sodium hydroxide (pH: 9), the second tank contains tap water, the third tank contains an acidic solution containing 2–4% Phosphoric acid (pH: 1), and the last two tanks contain demineralized water (conductivity: 6.7 $\mu\text{S}/\text{cm}$). The tanks were preheated to 60 °C. Glasses were first kept in the first tank for 9 min and then transferred to the second tank containing pure water. After the glasses were rinsed in the second tank and kept in the third tank for 9 min, they were rinsed in the second, fourth, and fifth tanks, respectively. The drying process was carried out by keeping it in the CRD-90 drying device (FinnSonic, Finland), at 100 °C for 8–10 min. These substrates were coated by the dip-coating method by KSV NIMA Dip Coater Single Vessel Medium (Biolin Scientific, Sweden) with a 150 mm/min pulling rate. As the cover glasses in Si-based PV panels bond to a polymeric phase (typically ethylene vinyl acetate), at this interface reflection losses are minimal and there is no AR application on this side. Therefore, to quantify the transmission gain from a single side coating we masked the rear faces of the glass substrates. After the coating step, the mask was removed, and the glass substrates were kept tilted at an angle of 10°–20° to the ground at room temperature. Following this step, the coatings were cured at 100 °C for 10 min in a PN200 oven (Carbolite, UK). The cured samples were heat treated at 700 °C in an AWF 12/25 furnace (Carbolite, UK) for 3 min, which is consistent with conventional thermal glass tempering conditions. Coated sample names were coded according to the molar ratio of MTES/TEOS as given in Table 1.

For the scale-up studies, an Easy Coater RCLM 1300 roller coating machine (Buerkle, Germany) was used, and 3.2 mm patterned glass panes were cut as (300 mm \times 400 mm) and the edges were ground to prevent damage to the rollers of the coating instrument. The coating machine has a rubber covered application roller with diameter of 240 mm and chromium plated doctor roller with diameter of 172 mm. The coating process was applied with a coating line speed of 5 m/min, application roller speed of 5 m/min, and doctor roller speed of

2 m/min. After samples were coated, they were cured at 100 °C for 1 min and tempered at 700 °C in a JetConvection tempering furnace (LandGlass Technology, China) for 3 min which are consistent with mass production conditions.

3 Characterization

Fourier transform infrared (FTIR) spectra (1765 measurement points with a resolution of 2 cm^{-1}) were recorded using a Bruker ALPHA FT-IR Spectrometer (Bruker, Germany) with a Platinum Attenuated Total Reflection (Platinum ATR) accessory in the range of 4000–500 cm^{-1} . The spectra of the silica structures produced with dual precursor chemistry were obtained for solutions in liquid phase at room temperature as well as for samples gelled at different temperatures. A Lambda 950 UV-Vis-NIR (Perkin Elmer, U.S.) spectrophotometer was used to determine the optical transmission of the samples coated with freshly prepared solutions in the range of 300–1100 nm. Additionally, to study the effect of aging on the solutions the average visible transmission ($T_{\text{vis}}\%$) of the samples coated with aged sols were measured to investigate the aging effects of solutions, according to the ISO 13468 standard method with the haze-gard I (BYK-Gardner Instruments, Germany) system. Transmission measurements were made with the D65 daylight illuminator. Optical haze measurements were done with the same instrument according to the ISO 14782 standard. Since samples were coated with the dip-coating method, each sample had coated and uncoated parts. Both full coated surfaces and the transition border between this region and the uncoated part were investigated using an Eclipse LV100POL (Nikon Corporation, Japan) optical microscope. The scanning electron microscopy (SEM) images were obtained with a Regulus SU8220 (Hitachi High-Tech Group, Japan) field emission-scanning electron microscope (FEG-SEM) for representative samples which are S0.3, S1.2, and S4.8. To investigate cross-sections, samples were prepared with a Hitachi IM4000 model ion milling unit. Furthermore, the sample which has optimum properties was examined with scanning transmission electron microscopy (STEM). Images were obtained with a FEI Tecnai TF20 instruments (Thermo Fisher Scientific, U.S.), working with an acceleration voltage of 200 kV. Sample preparation was carried out with a FEI Strata 400 (Thermo Fisher Scientific, U.S.) Focused Ion Beam/Scanning Electron Microscope (FIB/SEM). After the sample was coated with Pt and the cross-sections were prepared by focused ion beam (FIB) etching, the morphology of the samples was visualized by using Bright Field (BF) and High Angle Annular Dark Field (HAADF) STEM methods. All STEM analyses as well as the sample preparation steps were done externally by EAG laboratories. The hydrophobicity of the samples was determined by the surface contact angles of the coatings. The contact angles were

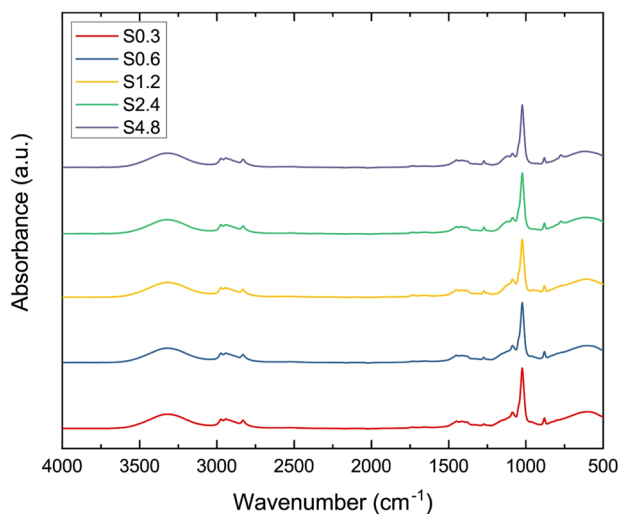


Fig. 2 FTIR spectra of coating sols between 4000 and 500 cm^{-1}

measured with the sessile drop method using a Theta Lite Optical Tensiometer (Biolin Scientific, Sweden) device by dropping 5 μl of distilled water on the surface. Moreover, the sample which has optimum properties was produced as prototypes of (300 mm \times 400 mm) and investigated mechanically in comparison with the uncoated reference sample in terms of EN 1096-2 and IEC 61215 standard methods.

4 Results and discussion

4.1 Fourier transform infrared (FTIR) spectroscopy

Alkoxysilane precursors were investigated in liquid phase sols with Fourier Transform Infrared (FTIR) spectroscopy. The FTIR spectra of the sols at room temperature show several bands corresponding to various chemical characteristics of networks between 4000 and 500 cm^{-1} (Fig. 2).

Peaks around 1000 cm^{-1} correspond to the stretching of Si–O bonds [23] and peaks in the range of 3000–3500 cm^{-1} represent O–H bonds [24]. These characteristic peaks were detected for each solution and do not serve as distinctive features. The region between 500 and 1500 cm^{-1} represents the fingerprint region of the IR spectrum and is separately plotted in magnified form to convey the differences between sols (Fig. 3).

Peaks around 1270 and 770 cm^{-1} become more pronounced with increasing MTES/TEOS molar ratio. The bonds corresponding to these peaks are due to Si–C and C–H bonds, respectively [25, 26]. These bonds are characteristic of the methyl group supplied by the MTES molecule.

On the other hand, the S1.2 composition was investigated with FTIR spectroscopy between 4000 and 500 cm^{-1} for the liquid sol as well as the hybrid silica gel samples

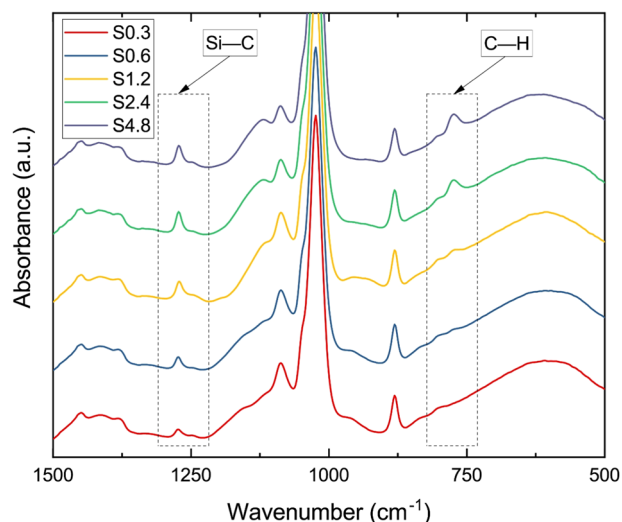


Fig. 3 Fingerprint region of FTIR spectra of coating solutions between 1500–500 cm^{-1}

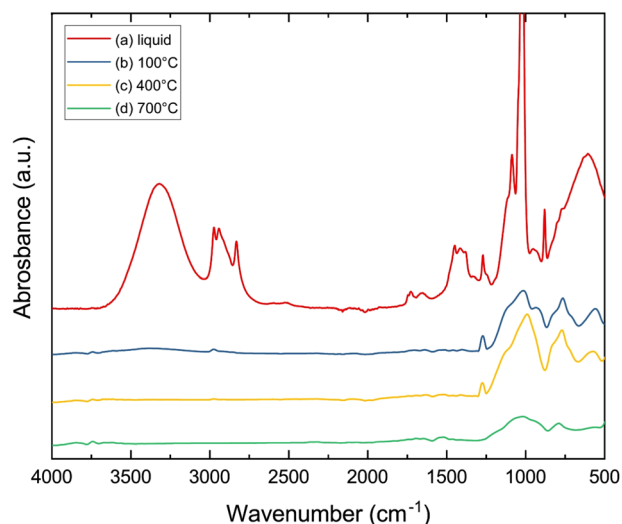


Fig. 4 FTIR spectra of S1.2 samples in (a) liquid phase and treated at (b) 100 °C, (c) 400 °C, (d) 700 °C between 4000 and 500 cm^{-1}

obtained by annealed at higher temperatures (100 °C, 400 °C, and 700 °C) (Fig. 4).

It is evident that the bonding chemistry is modified with temperature. The fingerprint region after zooming in is given in Fig. 5 to enable us to track the thermally induced changes in structural bonding.

Peaks of methyl groups were still observed in liquid solution and in solid gels that were exposed to 100 °C and 400 °C, but when exposed to 700 °C corresponding to tempering conditions, the Si–C peak around 1270 cm^{-1} almost completely disappeared. It was also observed that the intensity of the C–H peak around 770 cm^{-1} has decreased notably after heat treatment at increasing temperatures. These observations are consistent with previous studies which provide evidence for the pyrolysis of Si–CH₃

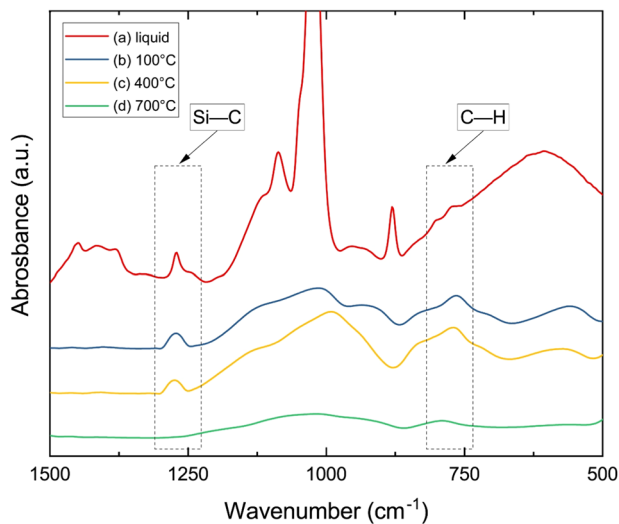


Fig. 5 Fingerprint region of FTIR spectra of S1.2 samples in (a) liquid phase, and treated at (b) 100 °C, (c) 400 °C, (d) 700 °C between 1500 and 500 cm^{-1}

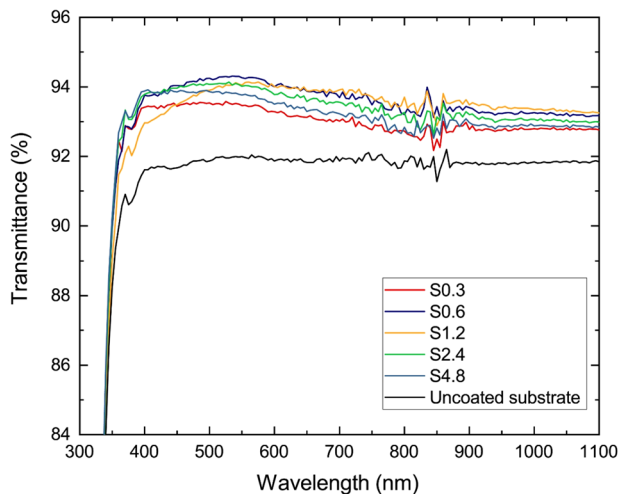


Fig. 6 Transmission spectrum of anti-reflective coated samples and uncoated substrates between 300 and 1100 nm

temperatures above 400 °C [26, 27]. Following pyrolysis, Si–OH bonds are likely to form and they would react to establish siloxane bonds at high temperatures [26].

4.2 Optical characterization

Optical characteristics of initial samples were examined with optical spectrophotometry between 300 and 1100 nm. Transmittance curves of samples that were coated with S0.3, S0.6, S1.2, S2.4, and S4.8 solutions were investigated in comparison with the uncoated substrate (Fig. 6). Single side coated glass samples exhibited overall transmittance gains around 2% within this range.

The coating procedure was repeated 1 day, 1 week, 2 weeks, and 7 weeks after the preparation date to

Table 2 Total visible transmission ($T_{\text{vis}}\%$) and haze (H%) values of samples which were coated with S0.3, S0.6, S1.2, S2.4, and S4.8 aged sols with different aging intervals

Aging Intervals	S0.3		S0.6		S1.2		S2.4		S4.8	
	T%	H%	T%	H%	T%	H%	T%	H%	T%	H%
Day 1	93.4	0.6	93.9	0.7	94.0	0.5	94.1	0.5	94.2	1.3
Week 1	93.8	0.5	94.3	0.7	94.4	0.5	93.6	0.5	93.2	1.1
Week 2	93.7	0.5	94.2	0.6	94.3	0.5	94.3	0.6	93.9	0.8
Week 7	93.4	0.6	94.0	1.2	94.2	0.6	94.1	0.6	93.8	1.4

investigate the effects of aging the sols on coatings and to estimate the stable shelf-life of the sols. 20 different samples were produced in total. Average transmission and haze measurements in the visible region were carried out following the heat treatment step (Table 2).

When the transmission values of the samples coated on the first day are examined, it is seen that the net transmission increases in parallel with the mole ratio of MTES/TEOS. Following subsequent coating, samples coated with S1.2 formulation showed the highest overall transmission values in a consistent manner. When the transmission values of the coated samples were re-measured after 1 week, it was observed that there was no significant change in the average transmission values in the visible range ruling out optical breathing triggered by water adsorption in the structural pores. The fact that visible transmission values up to 94.4% were obtained in these measurements show that chemical modification with the addition of MTES is persistent and the coated samples can withstand heat treatment at 700 °C without losing their AR properties (uncoated reference substrate had a transmission of 91.8%). Although haze values were acceptable for all samples, it was seen that the samples coated with the S1.2 coded sol have the most stable values which are close to the uncoated reference that has a haze value of 0.4%.

We also investigate the scalability of the proposed coating chemistry for use in an industrial setting. For this, we use the S1.2 sol as it stood out as the most stable composition. In the scale up studies, since the prototype samples (300 mm × 400 mm) were fully tempered which includes a heating-up and quenching stage, the finished samples could not be cut into small pieces to fit into the Lambda 950 spectrophotometer. Therefore, we used the haze-gard I device to investigate the optical transmission properties of these samples. These transmission measurements were done on five identically prepared samples. For each sample, the transmissions were acquired from nine different points that form a 3 × 3 grid on the substrates (Table 3). Intra sample measurements show that the AR coatings are homogeneous. The consistency of measurements among different samples additionally suggests that the proposed method is reproducible (Table 3).

4.3 Microscopic examinations

Altering sol composition to tune hydrophobicity inevitably affects the coating characteristics. In Fig. 7, optical microscopy images are given for the surface of the coatings produced with different sols. Additionally, images for two additional surfaces obtained by sols which represent the limiting cases of only TEOS (coded as T1) and only MTES (coded as M1) are also provided. We observe that coatings produced with MTES containing sols have frequent pin-hole defects throughout the surface due to the poorer wetting of the glass substrate.

As the glass substrates are partially dipped into the sols, a visual inspection of the coating borders is also possible. When the border lines are examined, it is seen that the T1 sample that was coated with solution including TEOS instead of MTES has a continuous coating border. Once MTES is added to the system the border becomes laden with pinned droplet formations whose diameters shrink with increasing

MTES ratio. It is known that methyl groups attached to an atom with low electronegativity will promote hydrophobicity [28]. Therefore, this trend is consistent with the increasing presence of MTES, which imparts a hydrophobic character to the sol. It is known that the presence of patterns may contribute to the self-assembly of liquid phases on such surfaces [29], and the presence of surface defects that modifies the wetting properties contribute to the formation of residual droplets and deformation of the meniscus [30]. In our case, there are no repeated surface features (protrusions or recessions) that would match the spatial periodicity of pinned droplets along the border line. The major factor that decides the border morphology seems to be the presence of the hydrophobicity promoting precursor MTES. We finally note that the resulting shape of the border has been long known to depend on the withdrawal speed and for a given solid-liquid combination there is a threshold speed below which the wetting (or in this case de-wetting) front is not deformed [31]. In the present study, the withdrawal speed is pre-fixed and it is dictated by the target thickness of the coating [32].

To understand the effect of the MTES molar ratio on the resulting coating thickness and layer structure, three representative cross-sectional images of the samples with the MTES/TEOS molar ratios that correspond to the case with least (0.3), medium (1.2), and maximum (4.8) MTES content, respectively, were examined with SEM analysis on samples prepared with ion milling (Fig. 8). It was observed that the coating thicknesses were 88 nm, 99 nm and 97 nm, respectively, and consistent with the basic quarter-wavelength recipe of AR coatings [1]. The SEM cross-section of a roll-coated sample shows a homogeneous layer with 103 nm thickness (Fig. 8d). The imaged layer has no structural differences from the dip-coated samples indicating that the proposed coating chemistry is scalable.

The observed thickness variations do not follow a monotonically increasing or decreasing trend with the alteration of

Table 3 Total visible transmission (T_{vis} %) values of samples which were coated by the roller coating machine using S1.2 solution

Measurement points	Samples				
	1	2	3	4	5
1	94.6	94.4	94.6	94.4	94.6
2	94.6	94.6	94.5	94.5	94.6
3	94.7	94.5	94.6	94.6	94.6
4	94.6	94.5	94.5	94.6	94.6
5	94.6	94.5	94.4	94.5	94.5
6	94.6	94.6	94.5	94.6	94.6
7	94.5	94.6	94.4	94.5	94.5
8	94.1	94.4	94.4	94.6	94.5
9	94.4	94.5	94.6	94.6	94.6
Average	94.5	94.5	94.5	94.5	94.6
Standard deviation	0.18	0.08	0.09	0.07	0.05

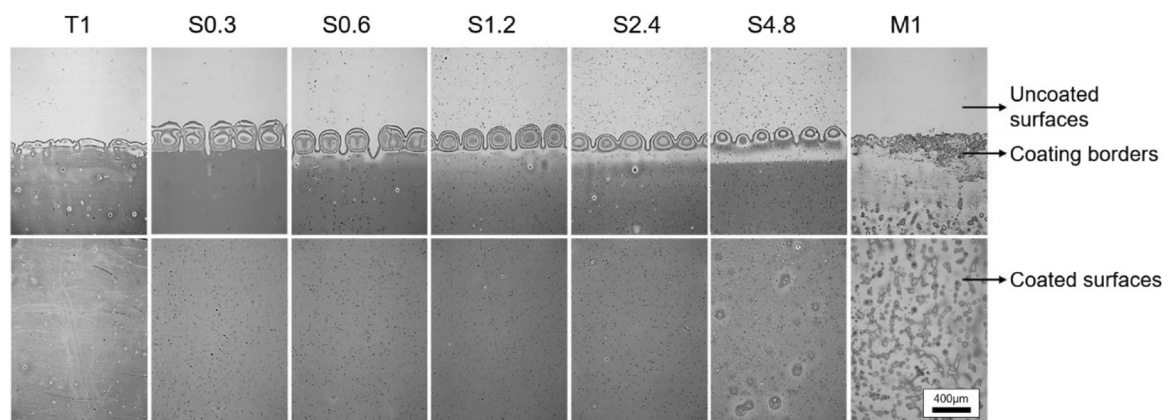
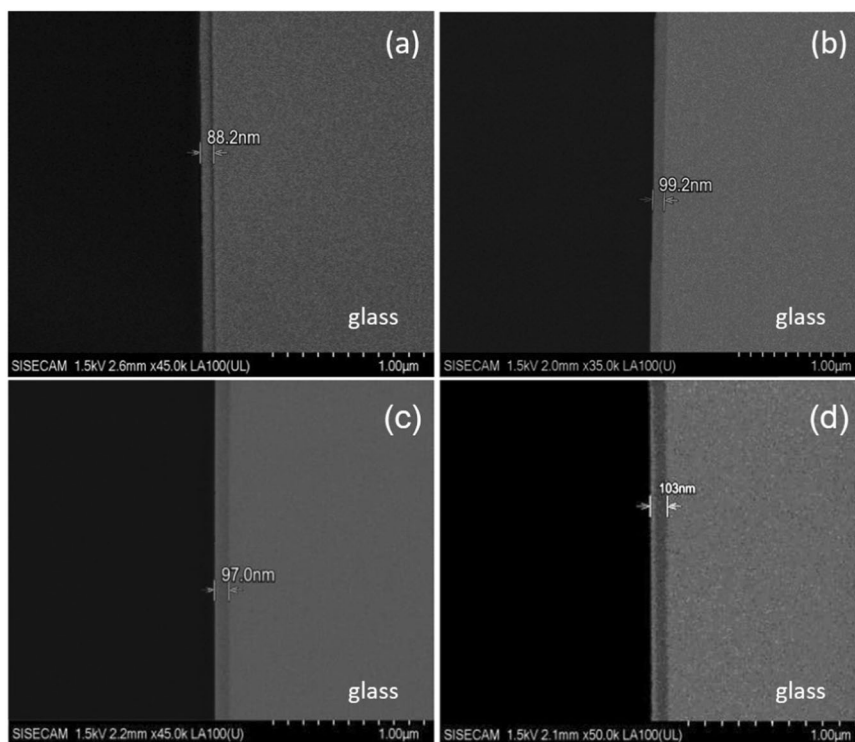


Fig. 7 Optical microscope images of coated samples by using 50X magnification. The darker shade regions correspond to the coated regions whereas regions with lighter shade pertain to the uncoated regions

Fig. 8 Cross-sectional scanning electron microscope (SEM) images of (a) S0.3, (b) S1.2, (c) S4.8 samples (d) S1.2 with roll coating



the MTES content of sols at a constant withdrawal speed. The structural pores are not directly visible through high resolution SEM analysis.

In order to examine the coating structure in detail, the cross-section of the S1.2 sample, which has the highest transmittance values and is closest to the ideal coating thickness, was additionally examined with a transmission electron microscope (Fig. 9). When the TEM images are examined, it is seen that the S1.2 sample thickness was approximately 100 nm and no distinct pore structure can be observed. The fact that no pores were found with this method, with which pores down to 2–3 nm in size could be detected, suggests that the reduction in effective refractive index is attained by pores with sub-nanometer size.

4.4 Surface wettability

Surface wettability of samples which were coated with S0.3, S0.6, S1.2, S2.4, and S4.8 solutions in different intervals were investigated with contact angle measurements. The droplet images of samples which were coated 1 day, 1 week, 2 weeks, and 7 weeks after the initial preparation of solutions are given in Fig. 10, and the measured contact angle values are given in Table 4. Columns represent solution codes and rows represent aging intervals.

It was observed that the contact angle value monotonically increased with increasing MTES/TEOS mole ratio for the samples coated on day 1. Similar trends were observed in the coatings produced in the following weeks

except for the sample S4.8 that is coated after 2 weeks. This exceptional case corresponds to a ratio of $\text{MTES/TEOS} = 4.8$ is likely to be stemming from the instabilities associated with sol aging due to the higher organic content. This unstable behavior is visually hinted by rampant coating inhomogeneities similar to those in Fig. 7 for S4.8. However, as expected, it was generally observed that increasing the MTES ratio in the solution translated into higher surface hydrophobicity.

4.5 Accelerated weathering tests

It has been found that samples coated with the S1.2 solutions had more stable properties than other formulations in terms of transmission values, surface wetting angles and coating thickness. This coating was also evaluated by EN 1096-2 and IEC 61215 standards to test against weathering effects. These standard test methods are used for coated glasses and solar modules, respectively, to predict long term performance under weathering conditions. Within the scope of this study, the IEC 61215 test was carried out specifically for the cover glass part of a PV module. Sample glasses were coated with S1.2 solution in prototype dimensions (300 mm × 400 mm) and tested simultaneously with the uncoated reference sample within the scope of these two standards. The EN 1096-2 standard includes condensation resistance, neutral salt spray resistance, acid resistance (SO_2), and linear abrasion resistance tests. S1.2 coated samples have

Fig. 9 Cross-sectional scanning transmission electron microscope (STEM) images of S1.2 sample in (a) BF-STEM and (b) HAADF-STEM modes

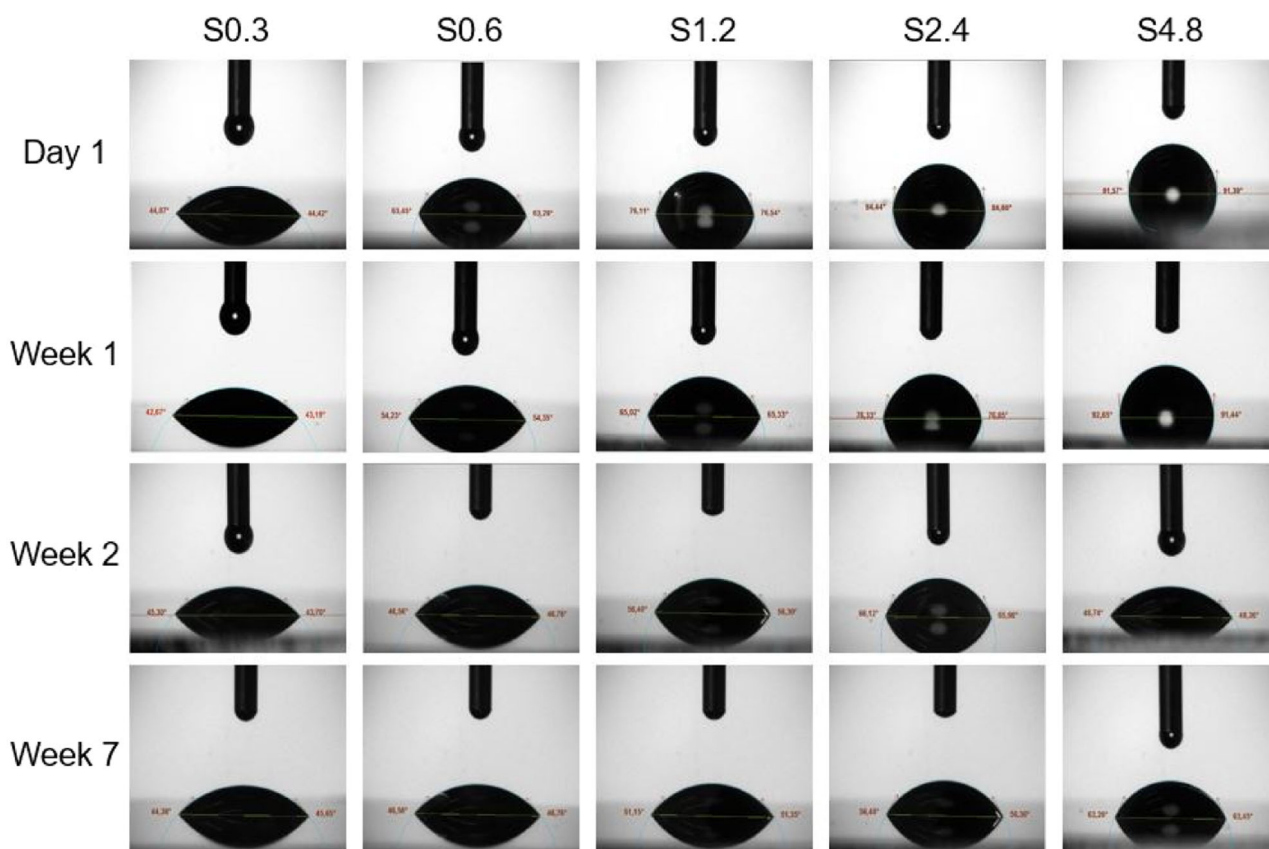
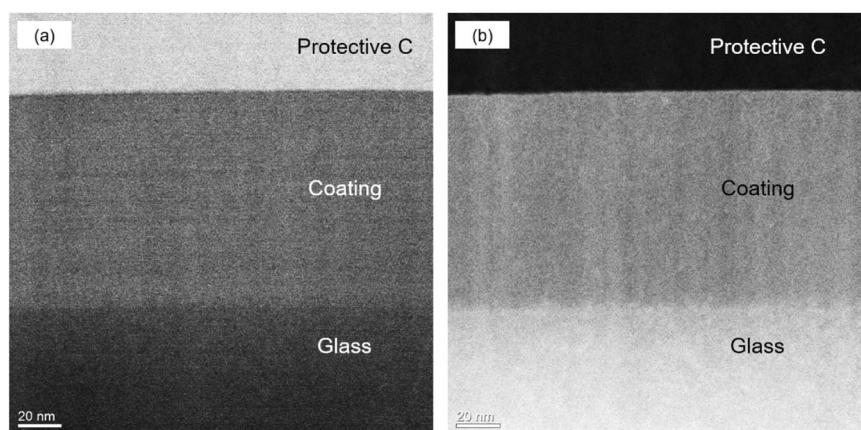


Fig. 10 Droplet images of samples which are coated with S0.3, S0.6, S1.2, S2.4, and S4.8 solutions after different solution aging intervals

successfully passed all these test groups as the transmission loss was consistently below 1% for each part. Additionally, glass samples were subjected to the IEC 61215 standard method which includes UV preconditioning, humidity freeze, thermal cycling, and damp heat tests. In order to evaluate the results of this test method, the difference between the pre-test and post-test transmittance values of coated glasses was compared. In UV preconditioning, damp heat, thermal cycling and humidity freeze tests, the transmission differences of S1.2

coated glasses were again found to be below 1%, whereas uncoated reference samples showed transmission gain exceeding 1% in damp heat test. This is thought to be due to the chemical corrosion and etching of the uncoated glass during testing and anti-reflective coated samples provide higher resistance in this particular case. Moreover, condensation and hazy appearance were observed on the uncoated sample surface after humidity freeze test, whereas this situation was not observed in S1.2 coated samples.

Table 4 Contact angle (CA°) values of samples which coated with S0.3, S0.6, S1.2, S2.4, and S4.8 solutions after different solution aging intervals

Aging Intervals	Contact Angle (CA°)				
	S0.3	S0.6	S1.2	S2.4	S4.8
Day 1	43.34	62.60	75.81	83.50	90.81
Week 1	42.81	58.50	67.00	81.79	91.86
Week 2	45.25	46.65	57.75	64.00	48.65
Week 7	44.50	46.50	51.00	56.00	63.00

5 Conclusion

In this study, we presented a comprehensive analysis of the preparation of thin-film coatings with a single step synthesis route using a hybrid chemistry which involved dual precursors MTES and TEOS in the presence of acid catalysis. The effects of changing MTES/TEOS mole ratios (0.3, 0.6, 1.2, 2.4, and 4.8) on the final properties of films were examined.

Even though the MTES component provides chemical durability and hydrophobicity as well as a process parameter to control the final thickness, after a critical level its over-presence adversely affects the adhesion strength and the overall stability of sols. Our key findings are as follows:

- Repeating the coating step with aged sols and monitoring the coating properties allowed us to identify the most stable composition as the one with the molar ratio of MTES/TEOS = 1.2.
- The precursors used in the proposed formulation are widely accessible common chemicals that are produced in mass quantities and the prepared sol can be used for up to 7 weeks with no adverse effects on optical performance (transmission and haze) and contact angle.
- The fact that no pores were directly visible in the TEM images despite the net transmission gain suggests a sub nanometer size nano-porous microstructure for the sample that has a molar ratio of MTES/TEOS = 1.2. After identifying the sol with a MTES/TEOS molar ratio of 1.2 as the optimal composition, we conducted a scalability study with an industrial grade roll coater on large substrates. These substrates were thermally tempered in a grade industrial furnace to mimic the serial production conditions. Optical performance measurements on the coated samples show that the developed coating chemistry can be directly scaled-up reproducibly without loss of performance. The cross-sectional SEM analysis also shows that the coatings attained by the roll coating process are homogeneous layers with comparable microstructural characteristics to the samples obtained by laboratory scale dip coating processes.

In conclusion, the inherent disadvantages of low chemical and physical resistance of anti-reflective coatings with open pore topology can be alleviated by a chemical modification with the addition of MTES to the coating sol. Following this modification, the final coatings can withstand very high annealing temperatures and maintain AR properties after weathering exposure.

Compliance with ethical standards

Conflict of interest The authors declare no competing interests.

Publisher's note Springer Nature remains neutral with regard to jurisdictional claims in published maps and institutional affiliations.

References

1. Hecht E (2017) Optics. 5th edn. Pearson Education, Harlow, Essex.
2. Glaser HJ (2000) Large area glass coating. Von Ardenne Anlagentechnik GMBH.
3. Chen D (2001) Anti-reflection (AR) coatings made by sol-gel processes: a review. *Sol Energy Mater Sol Cells* 68(3):313–336.
4. Glaubitt W, Löbmann P (2012) Antireflective coatings prepared by sol-gel processing: Principles and applications. *J Eur Ceram Soc* 32(11):2995–2999.
5. Ganjoo A et al. (2019) Glass and coatings on glass for solar applications. In: Musgraves JD, Hu J, and Calvez L (eds). Springer handbook of glass. Springer International Publishing, Cham. p. 1635–1676.
6. Yoldas BE (1980) Investigations of porous oxides as an antireflective coating for glass surfaces. *Appl Opt* 19(9):1425–1429.
7. Thomas IM (1986) High laser damage threshold porous silica antireflective coating. *Appl Opt* 25(9):1481–1483.
8. Thomas IM (1992) Method for the preparation of porous silica antireflection coatings varying in refractive index from 1.22 to 1.44. *Appl Opt* 31(28):6145–6149.
9. Xi JQ et al. (2007) Optical thin-film materials with low refractive index for broadband elimination of Fresnel reflection. *Nat Photonics* 1(3):176–179.
10. Xi JQ, Kim JK, Schubert EF (2005) Silica nanorod-array films with very low refractive indices. *Nano Lett* 5(7):1385–1387.
11. Guo Z et al. (2016) High-quality hollow closed-pore silica anti-reflection coatings based on styrene-acrylate emulsion @ organic-inorganic silica precursor. *ACS Appl Mater Interfaces* 8(18):11796–11805.
12. Du Y et al. (2010) Hollow silica nanoparticles in UV-visible antireflection coatings for poly(methyl methacrylate) substrates. *ACS Nano* 4(7):4308–4316.
13. Gao T, Jelle BP, Gustavsen A (2013) Antireflection properties of monodisperse hollow silica nanospheres. *Appl Phys A* 110(1):65–70.
14. Nielsen KH et al. (2014) Optical breathing of nano-porous anti-reflective coatings through adsorption and desorption of water. *Sci Rep.* 4(1):6595.
15. Cai S et al. (2014) Sol-gel preparation of hydrophobic silica antireflective coatings with low refractive index by base/acid two-step catalysis. *ACS Appl Mater Interfaces* 6(14):11470–11475.
16. Ma Y, Kanezashi M, Tsuru T (2010) Preparation of organic/inorganic hybrid silica using methyltriethoxysilane and tetraethoxysilane as co-precursors. *J Sol-Gel Sci Technol* 53(1):93–99.

17. Lin W et al. (2018) Characterization of sol-gel ORMOSIL anti-reflective coatings from phenyltriethoxysilane and tetraethoxysilane: microstructure control and application. *Surf Coat Technol* 345:177–182.
18. Chi F et al. (2020) Aggregation of silica nanoparticles in sol-gel processes to create optical coatings with controllable ultralow refractive indices. *ACS Appl Mater Interfaces* 12(14):16887–16895.
19. Muhammad AZ et al. (2021) Improved optical performance of hydrophobic silica nanoparticles as antireflection coating on glass and its electrical performance for photovoltaic module applications. *Optical Eng* 60(5):1–9.
20. Yoldas BE (1975) Alumina gels that form porous transparent Al_2O_3 . *J Mater Sci* 10(11):1856–1860.
21. Aydin G (2021) Tek katmanlı yansımaya önleyici ince film kaplamaların üretimi ve optik/mekanik özelliklerinin incelenmesi. İstanbul Technical University, Turkey.
22. Whitehouse D (2002) Surfaces and their measurement. Hermes Penton Science, London.
23. Pai PG et al. (1986) Infrared spectroscopic study of SiO_x films produced by plasma enhanced chemical vapor deposition. *J Vac Sci Technol A* 4(3):689–694.
24. Morrow BA (1990) Surface groups on oxides. In: Fierro JLG (ed) *Studies in surface science and catalysis*. Elsevier. p. A161–A224.
25. Zhao X et al. (2021) The influence of water content on the growth of the hybrid-silica particles by sol-gel method. *Silicon* 13(10):3413–3421.
26. Kamiya K et al. (1990) Thermal evolution of gels derived from $\text{CH}_3\text{Si}(\text{OC}_2\text{H}_5)_3$ by the sol-gel method. *J Non-Crystalline Solids* 121(1):182–187.
27. Yu S et al. (2003) The effect of TEOS/MTES ratio on the structural and dielectric properties of porous silica films. *J Electrochem Soc* 150(5):F116.
28. Koga Y et al. (2011) Is a methyl group always hydrophobic? Hydrophilicity of trimethylamine-n-oxide, tetramethyl urea and tetramethylammonium ion. *J Phys Chem B* 115(12):2995–3002.
29. Biebuyck HA, Whitesides GM (1994) Self-organization of organic liquids on patterned self-assembled monolayers of alkanethiolates on gold. *Langmuir* 10(8):2790–2793.
30. van Gestel MAC, He B, Darhuber AA (2020) Formation of residual droplets upon dip-coating of chemical and topographical surface patterns on partially wettable substrates. *Chem Eng Sci* 227:115832.
31. Blake TD, Ruschak KJ (1979) A maximum speed of wetting. *Nature* 282(5738):489–491.
32. Brinker CJ Dip coating. In: Schneller T et al. (eds.) *Chemical solution deposition of functional oxide thin films*. Springer Vienna, Vienna. p. 233–261.
33. Nečas D, Klapetek P (2012) Gwyddion: an open-source software for SPM data analysis. *Cent Eur J Phys* 10(1):181–188.